Journal of Advanced Ceramics
2024, **13**(11): 1881–1890
https://doi.org/10.26599/JAC.2024.9220976

Rapid Communication

Rapid fabrication of oxygen-deficient zirconia by flash sintering treatment

Xinghua Su[1,2,✉], Wenjin Li[1], Da Chen[3], Shuai Zhang[1], Chengguang Lou[1], Qiang Tian[2,✉], Jianguo Zhao[4], Peng Zhao[1,✉]

[1] *School of Materials Science and Engineering, Chang'an University, Xi'an 710061, China*
[2] *State Key Laboratory of Environment-Friendly Energy Materials, Southwest University of Science and Technology, Mianyang 621010, China*
[3] *School of Energy and Environment, Southeast University, Nanjing 210096, China*
[4] *School of Physics and Electronic Information, Luoyang Normal University, Luoyang 471022, China*

Received: July 28, 2024; Revised: September 6, 2024; Accepted: September 23, 2024

Abstract: The introduction of oxygen vacancies into zirconia is an effective strategy for enhancing its light absorption ability and photocatalytic performance. However, the cost-efficient preparation of oxygen-deficient zirconia (ZrO_{2-x}) remains challenging, which severely limits its broad application. In this study, flash sintering treatment was used to fabricate ZrO_{2-x} bulk in very short time of 90 s. Oxygen vacancies were introduced into ZrO_2 bulk through electrochemical reduction reactions. The as-prepared black ZrO_{2-x} exhibited excellent optical absorption capability, a small band gap (2.09 eV for direct and 1.67 eV for indirect), and a reduced conduction band energy, which is ascribed to the generation of oxygen vacancies and reduction of Zr cations. The as-prepared ZrO_{2-x} showed remarkable photocatalytic activity due to excellent solar light absorption and low recombination rate of electron–hole pairs. Flash sintering treatment provides a cost-efficient approach for rapidly fabricating ZrO_{2-x} bulk materials with high concentrations of oxygen vacancies, which can also be applied to other materials.

Keywords: zirconia; oxygen vacancy; flash sintering treatment; electrochemical reduction; optical absorption

1 Introduction

Solar energy has been an extraordinary source of renewable and green energy. With the ever-increasing demand for energy and concerns about the environment and climate, intensive studies have been conducted to develop photocatalytic materials for utilizing solar energy [1–4]. Owing to its high thermal stability, excellent mechanical properties, good resistance to corrosion, and low cost, zirconia (ZrO_2) has promising applications in the field of photocatalysis [5]. However, the wide band gap of zirconia (approximately 5–6 eV) enables it to absorb only ultraviolet light (< 248 nm), resulting in low efficiency in solar energy harvesting, which severely restricts its development in photocatalysis [6–8]. Therefore, efforts should be made to reduce the band gap of zirconia in an attempt to extend the optical absorbance from the ultraviolet region to the visible and near-infrared regions.

The introduction of oxygen vacancies through doping and partial reduction has been demonstrated to be an effective method to reduce the band gap of metal oxide semiconductors [9–12]. This modification leads to the generation of mid-gap states between the valence and conduction bands [13–15]. Consequently, the band gap of a metal oxide semiconductor can be narrowed. For example, the band gap of titania (TiO_2) can be reduced from 3.10 to 1.99 eV by increasing the oxygen vacancy content [12]. Nevertheless, it is challenging to generate oxygen vacancies in zirconia because of the high oxygen vacancy formation energy (approximately 9 eV) [16,17]. Thus, some more drastic conditions are employed to introduce oxygen vacancies into zirconia and prepare oxygen-deficient zirconia (ZrO_{2-x}). For example, Dashtbozorg *et al.* [16] applied a low-pressure (300 Pa) plasma treatment (H_2 gas at 500 °C for 5 h) to prepare ZrO_{2-x} bulk materials. Zu *et al.* [18] presented a molten lithium reduction approach to prepare black ZrO_{2-x} powders at 400 °C under high-purity argon gas. However, the sample should be washed repeatedly with HCl solution, deionized water, and ethanol to thoroughly remove impurities. Wang *et al.* [19] used a high-pressure (6 GPa) torsion method to produce black ZrO_{2-x} material with a disc shape. Although these methods can effectively reduce the band gap of zirconia and prepare black ZrO_{2-x}, the preparation processes are complicated, and harsh processing conditions, such as high temperatures and pressures, are required, which are not conducive to industrial production. Consequently, significant efforts should be dedicated to developing simple and cost-effective methods for producing black ZrO_{2-x}.

Flash sintering is a novel electric field/electric current-assisted sintering method presented by Raj *et al.* in 2010 [20], which has the advantage of rapid densification in several seconds at temperatures much lower than conventional sintering temperatures [21–25]. The unique characteristic of flash sintering is the direct application of an electric field to the sample. The current increases rapidly to a limited value when the sample is heated to a specific temperature because of the negative temperature coefficient of resistivity. As a current passes through a

✉ Corresponding authors.
E-mail: X. Su, suxinghua@chd.edu.cn;
Q. Tian, tqsuperego@163.com;
P. Zhao, zyzhaop@chd.edu.cn

sample, the phenomenon of electrochemical reduction is observed during flash sintering, which starts from the cathode, where the electrons are injected into the sample from the metal electrode [26–34]. The oxygen vacancies are generated in the electrochemical reduction process, which is proposed to be responsible for the increased electronic conductivity and enhanced diffusion kinetics. According to reported studies in the literature, the electrochemical reduction reaction that occurs during flash sintering can produce oxygen vacancies, which provides an alternative way to prepare oxygen-deficient zirconia ZrO_{2-x}.

In this study, flash sintering treatment was first employed to prepare ZrO_{2-x} bulk samples with high concentrations of oxygen vacancies, which exhibited excellent optical absorption capability due to their small band gap. Moreover, the as-prepared ZrO_{2-x} shows remarkable photocatalytic activity.

2 Experimental

2.1 Sample preparation

Commercially, 5 mol% yttria-stabilized zirconia (5YSZ) bulk samples (5 mm × 5 mm × 2 mm) with a relative density of 99% were used as starting samples. Prior to flash sintering treatment, the samples were first ground with 4000-grit silicon carbide abrasive paper and then polished with a diamond suspension. After that, ultrasonic cleaning was performed for 10 min to remove contaminants. The setup used for flash sintering treatment is schematically shown in Fig. 1. The sample was sandwiched between platinum sheet electrodes with a thickness of 0.2 mm. To ensure close contact between the sample and the electrode, a load of approximately 1 MPa was applied to the electrodes through the alumina plates and rods (Fig. S1 in the Electronic Supplementary Material (ESM)). The platinum sheet electrodes and the direct current power supply (HPS0614, Hangzhou Lanyi Electronics Co., Ltd., China) were connected through platinum wires to apply a constant voltage of 30 V to the sample. A digital multimeter (DMM 4040, Tektronix, USA) was used to record the voltage and current. The flash sintering treatment process was carried out in a furnace at a heating rate of 10 °C/min under an air atmosphere. When the sample was heated to a specific temperature, the current flowing through the sample increased abruptly to a limit value of 2.5 A. The sample was then kept at a constant current of 2.5 A for 90 s. Finally, the power supply and furnace were cut off, and the sample was naturally cooled down to room temperature.

2.2 Sample characterizations

An X-ray diffractometer (XRD; D8 Davinci, Bruker, Germany) with Cu Kα radiation was used to identify the crystallographic phase of samples. Raman spectra of the samples were collected on a Raman spectrometer (JY HR800, Horiba Jobin Yvon, France) with 532 nm diode laser excitation. Electron paramagnetic resonance (EPR) spectroscopy was conducted on a A300 spectrometer (Bruker, Germany) at room temperature to determine the number of oxygen vacancies in the samples. The chemical composition of samples was analyzed by X-ray photoelectron spectroscopy (XPS) using an ESCALAB 250 spectrometer (Thermo VG Scientific, USA) with monochromatic Al Kα excitation. The morphology of flash-treated samples was observed by a field emission scanning electron microscope (SEM; S-4800, Hitachi, Japan). The microstructure of flash-treated samples was investigated using a scanning transmission electron microscope (STEM; Talos F200X G2, Thermo Fisher Scientific, USA). The foils used for STEM were prepared with a focused ion beam (FIB). The electrical conductivity of samples was tested using the DC four-probe method. A digital multimeter (DMM 4040, Tektronix, USA) with high precision was used for the DC four-probe measurement. The diffuse reflectance spectra were measured on an ultraviolet–visible–near infrared (UV–VIS–NIR) spectrophotometer (UV-3600, Shimadzu, Japan) in the wavelength range of 250–2500 nm.

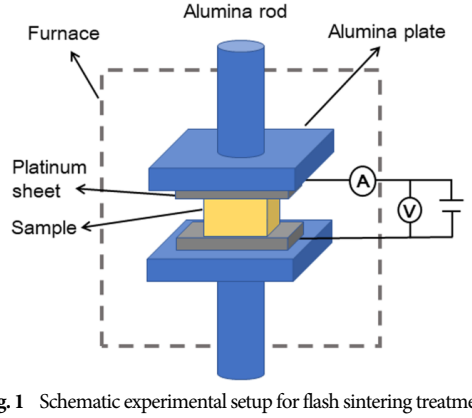

Fig. 1 Schematic experimental setup for flash sintering treatment.

2.3 Photocatalytic activity evaluation

The photocatalytic activity of samples was evaluated via the degradation of methylene blue (MB) under visible light using 300 W xenon lamps as the light source. 50 mg of sample was immersed in 100 mL of MB solution at a concentration of 5 mg/L. The MB solution was continuously stirred, and the temperature was maintained at 25 °C with a water circulation instrument. Prior to illumination, the MB solution containing the sample was kept in the dark for 30 min to ensure adsorption-desorption equilibrium between the sample and solution. During the exposure, 5 mL of MB solution was regularly taken out at time intervals of 20 min. The solution was measured by a UV–VIS spectrophotometer (1901PC; Shanghai Lengguang Technology, China). The degradation efficiency (η) of MB can be calculated using the Lambert–Beer law (Eq. (1)):

$$\eta = \left(1 - \frac{c_t}{c_0}\right) \times 100\% = \left(1 - \frac{A_t}{A_0}\right) \times 100\% \quad (1)$$

where c_0 and c_t represent the initial and final concentrations of MB, respectively, and A_0 and A_t represent the initial and final absorbance at the characteristic wavelength of 663 nm, respectively.

3 Results and discussion

The current density and power dissipation of samples as a function of the furnace temperature during the flash sintering treatment are shown in Fig. 2. The current density (J) and power dissipation (W) are calculated by Eqs. (2) and (3):

$$J = \frac{I}{S} \quad (2)$$

$$W = \frac{UI}{V} \quad (3)$$

where I is the current flowing through the sample; S is the surface area between the sample and electrode (25 mm^2); U is the applied voltage; V is the volume of the sample (50 mm^3). The abrupt rise in the current density at approximately 568 °C indicates the occurrence of flash sintering (or flash events) [35,36].

Nevertheless, the actual sample temperature in the flash furnace is higher than the furnace temperature of 568 °C because of Joule heating, which is estimated to be 791 °C using the black body radiation theory [37]. When the current density reaches the limit value of 10 A/cm^2, the sample is kept for 90 s at a constant current density, as shown in Fig. 2(a). The occurrence of flash events is also confirmed by the nonlinear increase in the power dissipation (Fig. 2(b)) [38,39], implying a non-linear rise in electrical conductivity of the sample. Furthermore, the transition from linear to non-linear in the Arrhenius plot occurs at a power dissipation of approximately 35 mW/mm^3, which is consistent with the reported works [40,41]. This result indicates that Joule heating plays a critical role in inducing flash events.

Figure 3 shows photographs of the samples before and after flash sintering. Clearly, the color of the sample completely changes from white to black, indicating that the optical absorption ability of the sample is greatly improved after the flash sintering treatment. Moreover, a gradient of blackening is observed from the cross-sectional view, with a darker color near the cathode, as shown in Fig. 3(d). This result suggests that the blackening is initiated at the cathode and propagates toward the anode, which is similar to other electrochemical reduction methods [16,30]. The color change from white to black clearly indicates that oxygen vacancies are introduced into the sample and that oxygen-deficient zirconia is successfully prepared. However, more direct evidence is needed to confirm the generation of oxygen vacancies during flash sintering.

To study the phase stability of samples after flash sintering, the crystalline structures of the untreated and flash-treated samples were measured via XRD, as shown in Fig. 4(a). Both the XRD patterns of the white sample (before flash) and black sample (after flash) can be indexed as tetragonal phase zirconia (PDF#80-0784), revealing that the crystalline structure of the sample remains after the flash sintering treatment. Moreover, no secondary phase or peak shift was detected, indicating that flash sintering treatment cannot induce the formation of a secondary phase in the sample.

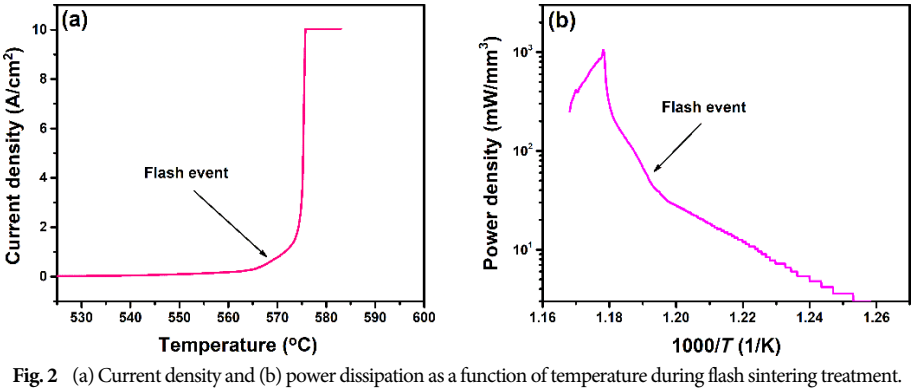

Fig. 2 (a) Current density and (b) power dissipation as a function of temperature during flash sintering treatment.

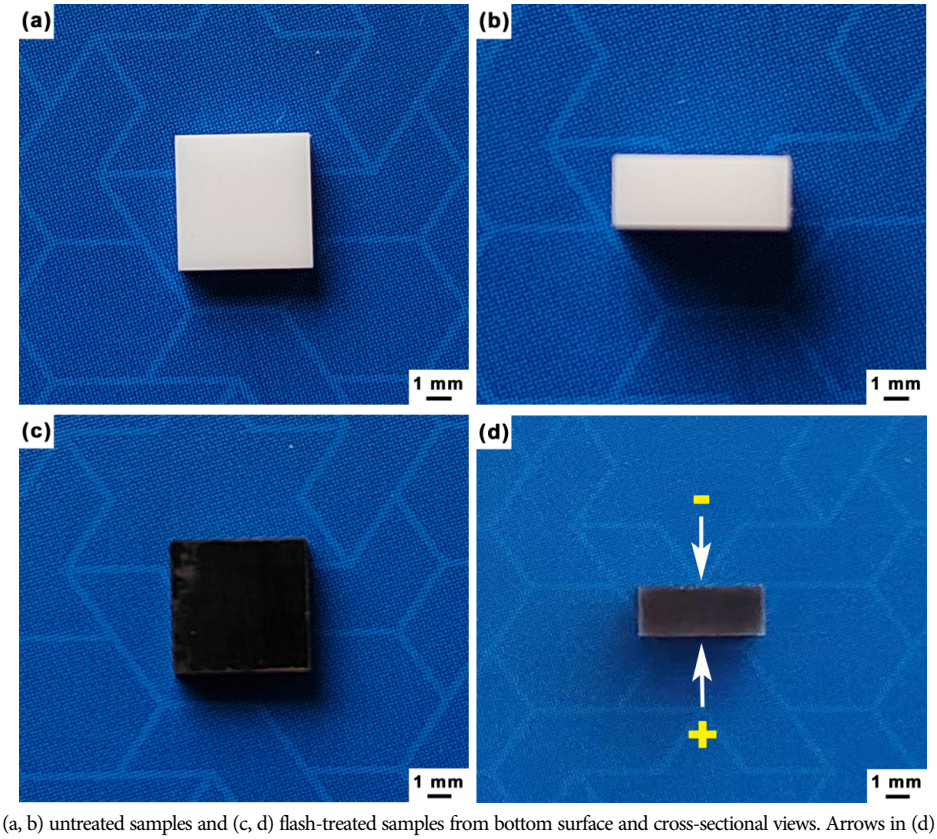

Fig. 3 Photographs of (a, b) untreated samples and (c, d) flash-treated samples from bottom surface and cross-sectional views. Arrows in (d) indicate sample surfaces facing anode and cathode.

清華大学出版社 Tsinghua University Press | SciOpen

The lattice parameters of the untreated and flash-treated samples (Table 1) were calculated by Rietveld refinement using the FullProf software (Fig. S2 in the ESM). The lattice parameters and unit cell volume decrease after flash treatment, which is attributed to the formation of oxygen vacancies in the samples.

The Raman spectrum is very sensitive to lattice rearrangement and disorder. Accordingly, the samples before and after flash sintering treatment were further characterized via Raman spectroscopy. As shown in Fig. 4(b), both samples exhibit 6 Raman-active vibrational modes (A_{1g}+$2B_{1g}$+$3E_g$) of tetragonal zirconia belonging to the *P*42/*nmc* space group [42]. The observed bands are assigned as follows: A_{1g} at 605 cm^{-1}, B_{1g} at 147 and 318 cm^{-1}, and E_g at 260, 463, and 642 cm^{-1} [42–44]. The samples before and after flash treatment had similar Raman spectra, indicating that no significant long-range distortion of the lattice occurs during the flash sintering treatment. Nevertheless, the Raman spectra show a decreased intensity after the flash, which is attributed to the generation of oxygen vacancies and a disordered microstructure [45].

Electron paramagnetic resonance (EPR) spectroscopy is a commonly used method to identify paramagnetic F^+ centers ($V_O^{\cdot}$) with single trapped electrons and can be used to evaluate the concentration of oxygen vacancies [46–48]. Therefore, EPR was conducted to confirm the introduction of oxygen vacancy defects by the flash sintering treatment. Figure 5 shows the EPR spectra of the untreated and flash-treated samples. Both samples exhibit similar EPR signals (g = 2.003), which is ascribed to the unpaired electrons localized in the oxygen vacancies, revealing the existence of oxygen vacancies in both samples [46,47]. However, compared with that of the untreated sample, the EPR signal intensity of the flash treated sample is higher, indicating that flash sintering treatment introduces more oxygen vacancies into the sample. Moreover, the current density has a significant influence on the number of oxygen vacancies during the flash treatment. The larger current density helps introduce the higher concentration of oxygen vacancy defects into the sample (Fig. S3 in the ESM). However, large currents will cause the formation of hot spots, leading to cracks in the sample (Fig. S4 in the ESM). Therefore, the current limit should be optimized in the flash treatment of a sample.

To further quantitatively estimate the concentration of oxygen vacancies, XPS analysis was conducted. The high-resolution Zr 3d XPS spectrum of the untreated sample (Fig. 6(a)) shows two peaks at 181.5 and 183.9 eV, corresponding to the $3d_{5/2}$ and $3d_{3/2}$ electron states, respectively [49]. This spectrum can be deconvoluted into four fitting peaks, which can be ascribed to Zr^{4+} at 181.7 and 184.0 eV and Zr^{3+} at 181.4 and 183.8 eV [50,51]. For the flash-treated sample, in addition to the Zr $3d_{5/2}$ and Zr $3d_{3/2}$ peaks at 181.5 and 183.9 eV, a small peak at 178.7 eV appears, which can be assigned to the lower valence state of Zr cations in ZrO_{2-x} [52,53]. Furthermore, the fitted peaks of Zr^{4+} and Zr^{3+} do not significantly shift, with binding energies of 181.7 and 184.1 eV, and 181.5 and 183.9 eV, respectively. However, the intensities of the Zr^{4+} fitting peaks become weaker, whereas the intensities of the Zr^{3+} fitting peaks become stronger, as depicted in Fig. 6(b). These results suggest that the proportion of Zr^{3+} is significantly increased after the flash sintering treatment. The normalized compositions of the fitted components of the samples before and after flash sintering treatment are given in Table 2. The proportion of Zr^{3+} is increased from 3.86% to 58.96% at the surface of the sample after the flash sintering treatment. Moreover, the proportion of Zr^{4+} decreases from 96.14% to 33.23%.

The O 1s XPS spectra of the samples before and after flash sintering treatment are shown in Figs. 6(c) and 6(d). Three fitting peaks located at 528.6, 530.0, and 531.2 eV are attributed to lattice oxygen (O_L), oxygen vacancy (O_V), and adsorbed oxygen (O_C), respectively [54,55]. The intensity of the O_V fitting peak becomes stronger after the flash sintering treatment, implying the introduction of oxygen vacancy defects. As depicted in Table 2, the proportion of O_V component is increased from 26.12% to 38.03%, whereas the proportion of O_L component is decreased from 59.55% to 48.72%. Notably, O_V in the untreated sample is resulted from the addition of yttria to zirconia. Apparently, it can be concluded that oxygen vacancies are introduced by the flash sintering treatment according to the XPS results.

The microstructure of the flash-treated sample was investigated using SEM and STEM. Figure 7(a) shows an SEM image of a flash-treated sample. A dense structure without pores can be observed, indicating that the pores are not formed in the sample after the flash treatment. However, the bright-field transmission electron microscopy (TEM) image reveals the existence of subgrains, as shown in Fig. 7(b). Furthermore, high-density dislocations and stacking faults can be observed in the STEM image shown in Fig. 7(c). These results reveal that flash treatment has a significant

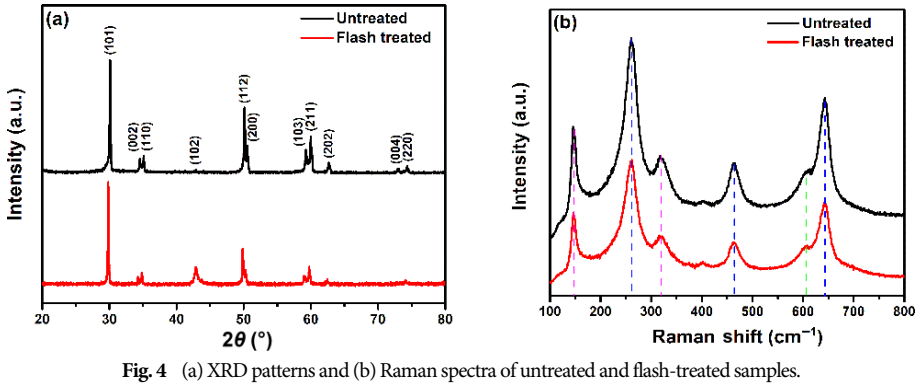

Fig. 4 (a) XRD patterns and (b) Raman spectra of untreated and flash-treated samples.

Table 1 Lattice parameters of samples before and after flash sintering treatment

Sample	Phase	*a* (Å)	*b* (Å)	*c* (Å)	*V* (Å^3)
Untreated	Tetragonal	3.59967	3.59967	5.16919	66.980
Flash treated	Tetragonal	3.59619	3.59619	5.16485	66.795

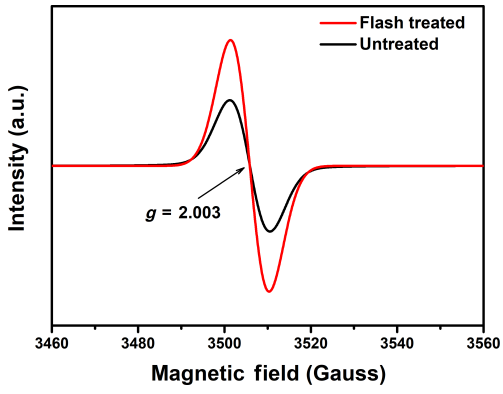

Fig. 5 EPR spectra of untreated and flash-treated samples.

effect on the microstructure of the sample. Subgrains with grain boundaries and defects such as dislocations and stacking faults are generated during flash treatment, which are helpful to improve the mechanical properties [56,57].

In the flash sintering treatment, a reversible electrochemical reaction occurs at the interface between the zirconia sample and the platinum electrode, as described by Reaction (4) [26]:

$$O_O^X \leftrightarrow V_O^{\cdot\cdot} + 2e' + \frac{1}{2}O_2 \quad (4)$$

Since the electrons move toward the anode under the electric field, oxygen vacancies ($V_O^{\cdot\cdot}$) are generated at the anode according to the forward reaction in Reaction (4); thus, the anode acts as a source of oxygen vacancies. The oxygen vacancies drift toward the cathode under an electric field, and the reverse reaction in Reaction (4) occurs. Then, the oxygen vacancies are annihilated by absorbing oxygen from the atmosphere, and electrons are injected from the cathode. If the amount of oxygen entering the cathode is less than the amount of oxygen leaving the anode, electrochemical reduction occurs according to Reaction (5):

$$xV_O^{\cdot\cdot} + ZrO_2 + 2xe' \rightarrow ZrO_{2-x} + xO_O^X \quad (5)$$

where x represents the amount of oxygen vacancies in partially reduced zirconia. This electrochemical reduction reaction results in the formation of oxygen-deficient zirconia (ZrO_{2-x}) with black color, which is also called electrochemical blackening [58]. This phenomenon develops from the cathode and migrates to the anode, which is consistent with the darker color near the cathode (Fig. 3(d)). In addition, the trapping of electrons at Zr^{4+} leads to the formation of Zr^{3+} and even a lower valence state of Zr cations [53,58], as shown in Fig. 6(b).

The optical absorption properties of the untreated and flash-treated samples were investigated using the UV–VIS–NIR diffuse reflectance spectroscopy (250–2500 nm), as displayed in Fig. 8. The white-colored untreated sample exhibits strong optical absorption in the UV region. Moreover, it has fairly low absorbance in the VIS–NIR region. These results are attributed to the relatively large band gap of the sample [16]. In contrast, flash-treated samples with a black color exhibit excellent optical absorption capability (> 92%) in the full spectral region, which is greater than that of ZrO_{2-x} prepared via conventional methods [16–18]. Apparently, the optical absorption ability of the sample is significantly enhanced by the flash sintering treatment. Owing to its excellent optical absorption capability across the entire solar spectrum, ZrO_{2-x} has important applications in the field of solar energy harvesting. The greatly enhanced optical absorption capability of ZrO_{2-x} is ascribed to the decreased bang gap due to the presence of highly concentrated oxygen vacancies and the low valance state of Zr cations. It has been reported that the electronic band structure of metal oxides can be modified by the introduction of oxygen vacancy defects and low-valence state cations, which leads to the formation of mid-gap states within the intrinsic band gap. These mid-gap states extend to and overlap with the edge of the conduction band, thus resulting in a reduced bandgap [12,46,48].

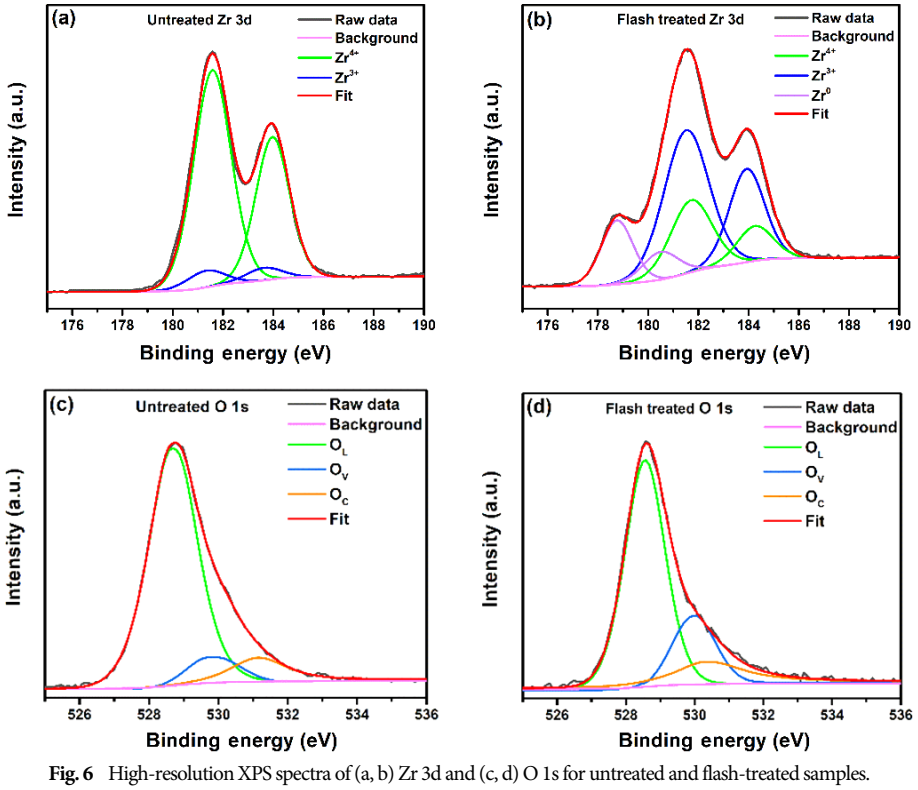

Fig. 6 High-resolution XPS spectra of (a, b) Zr 3d and (c, d) O 1s for untreated and flash-treated samples.

Table 2 Normalized compositions of fitted components for samples before and after flash sintering treatment

Component	Composition (%)	
	Before flash	After flash
Zr^{4+}	96.14±0.01	33.23±0.01
Zr^{3+}	3.86±0.01	58.96±0.01
Zr^{0}	0.00	7.81±0.01
O_L	59.55±0.02	48.72±0.03
O_V	26.12±0.02	38.03±0.02
O_C	14.33±0.03	13.25±0.03

The direct and indirect band gaps of the untreated and flash-treated samples are calculated on the basis of UV–VIS–NIR reflection spectra using the Tauc method and Kubelka–Munk function [59], as shown in Figs. 9(a) and 9(b). The white-colored untreated sample has a direct band gap of 4.18 eV and an indirect band gap of 2.85 eV. After the flash treatment, the direct band gap and indirect band gap are decreased to 2.09 and 1.67 eV, respectively. The significant decrease in the band gap is attributed to the formation of oxygen vacancies and the low valance state of Zr cations [17,18]. Furthermore, the valence band positions of the untreated and flash-treated samples were determined from the valence band XPS spectra. As displayed in Fig. 9(c), the top edges of the valence band for the untreated and flash-treated samples are 2.41 and 2.08 eV, respectively.

Combining the valence band (VB) positions and the band gap values, the energy band diagrams of the untreated and flash-treated samples were constructed, as depicted in Fig. 10. The bottom edge of the conduction band (CB) for the untreated sample is calculated to be −1.77 eV (direct) and −0.44 eV (indirect), while it is calculated to be −0.01 eV (direct) and 0.41 eV (indirect) for the flash-treated sample. Obviously, the top edge of the valence band of the sample increases by −0.33 eV after flash treatment. Moreover, there is a decrease in the bottom edge of the conduction band (1.76 eV for direct and 0.85 eV for indirect) after flash treatment. These results indicate that the Fermi energy level shifts toward the conduction band, suggesting the creation of new donor energy levels close to the conduction band due to the formation of oxygen vacancies and the reduction of Zr cations [60,61]. As a result, the black ZrO_{2-x} ceramics shows a higher electrical conductivity of 560 mS/cm compared to the white ZrO_2 ceramics (27 mS/cm).

Compared with the conventional methods for preparing ZrO_{2-x}, flash sintering treatment has the advantages of rapid fabrication, simple processing and equipment, and environmentally friendly production. By adjusting various flash treatment parameters, such as electric field, current limit, temperature, and holding time at constant current, the amount of oxygen vacancies and degree of reduction of Zr cations can be controlled, thus tailoring the band structure and optimizing the physical and chemical properties of zirconia. For example, n-type or p-type semiconducting zirconia can be potentially prepared by the flash sintering treatment. Furthermore, flash sintering treatment can be applied to implant oxygen vacancies to other materials, opening new avenues for the development and production of innovative materials.

The photocatalytic ability of the as-prepared ZrO_{2-x} was evaluated by choosing the degradation of pollutant dyes such as

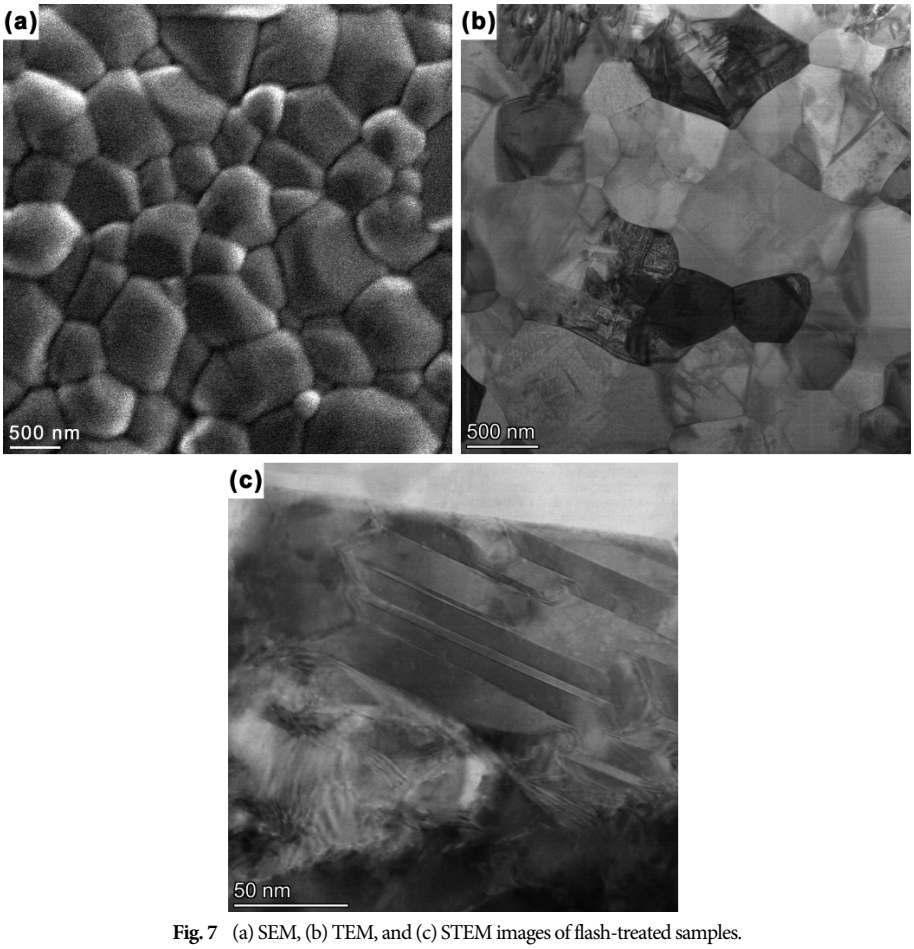

Fig. 7 (a) SEM, (b) TEM, and (c) STEM images of flash-treated samples.

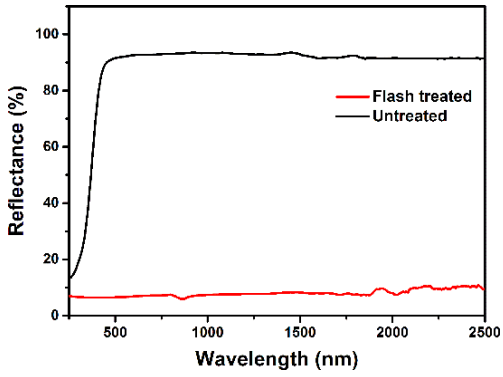

Fig. 8 UV–VIS–NIR diffuse reflectance spectra of untreated and flash-treated samples.

MB in the presence of simulated solar light (300 W xenon lamps). Figures 11(a) and 11(b) show the UV–VIS absorbance patterns of the MB solution during the photocatalytic process. The absorption peak intensity reaches a maximum at a wavelength of 663 nm for the untreated and flash-treated samples, which is in accordance with the reported works on the degradation of MB [17,62]. Moreover, the UV–VIS absorbance curves show a continuous decreasing trend with the increase of irradiation time for both samples, indicating that the MB is gradually removed from the solution with increasing irradiation time. In addition, the UV–VIS absorbance curve of the solution kept in the dark for 30 min overlaps with that of the initial MB solution for the untreated sample, as shown in Fig. 11(a). This result suggests that the untreated sample has no good adsorption capacity for MB. However, the adsorption capacity of a sample can be improved by the flash sintering treatment. Figure 11(b) shows that there is a decrease in the intensity of the absorption curve after the MB solution is kept in the dark for 30 min for the flash-treated sample.

According to the Lambert–Beer law and the absorbance at the characteristic wavelength of 663 nm [62], the photocatalytic degradation efficiency can be obtained. Figure 11(c) displays the

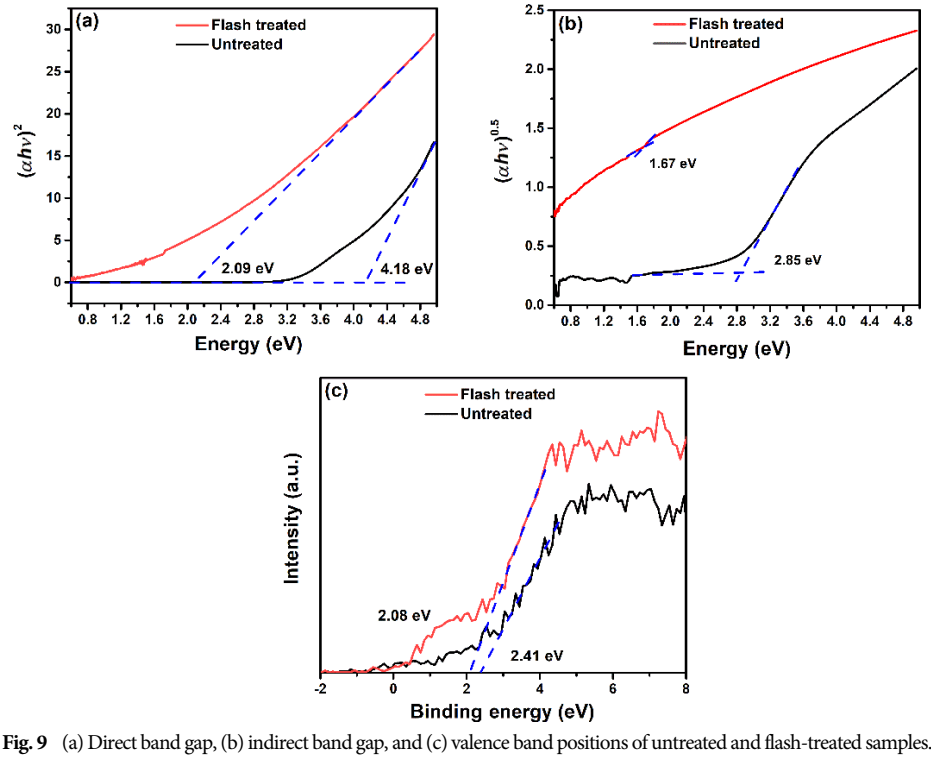

Fig. 9 (a) Direct band gap, (b) indirect band gap, and (c) valence band positions of untreated and flash-treated samples.

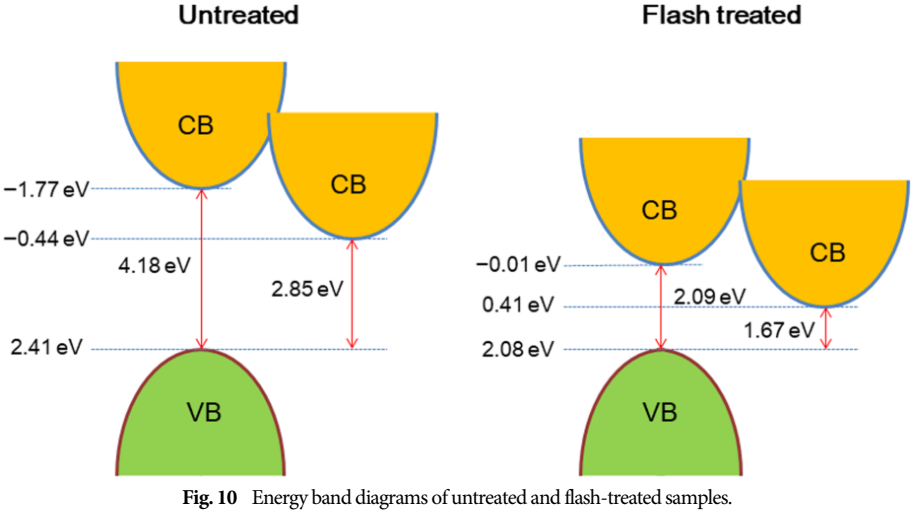

Fig. 10 Energy band diagrams of untreated and flash-treated samples.

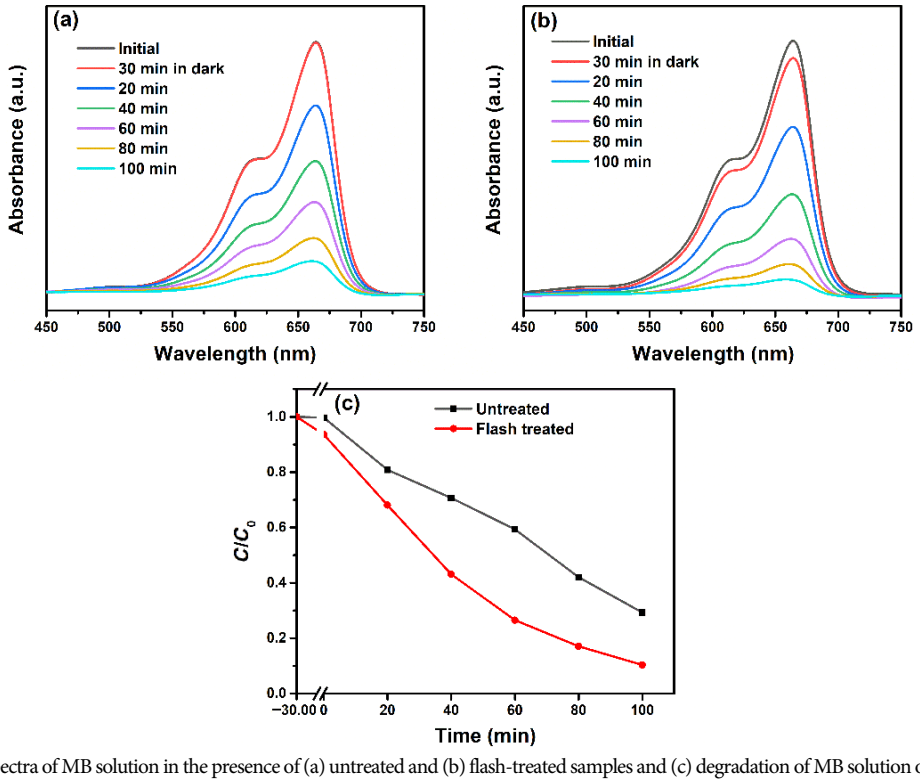

Fig. 11 UV–VIS spectra of MB solution in the presence of (a) untreated and (b) flash-treated samples and (c) degradation of MB solution over irradiation time.

plots of the MB concentration ratio versus irradiation time for the untreated and flash-treated samples. The degradation efficiency of the MB solution is approximately 70.39% after 100 min for the untreated sample. However, the degradation efficiency can reach 89.65% after 100 min for the flash-treated sample ZrO_{2-x}. These results clearly reveal that ZrO_{2-x} has an enhanced photocatalytic ability compared with ZrO_2. These findings suggest that the remarkable photocatalytic activity of ZrO_{2-x} is mainly due to the enhanced solar light absorption. Furthermore, the recombination rate of electron–hole pairs is reduced due to the presence of Zr^{3+} ions in ZrO_{2-x} [63], which is also beneficial for photocatalytic activity.

4 Conclusions

Oxygen-deficient zirconia (ZrO_{2-x}) bulk materials with black color were successfully fabricated by flash sintering treatment for a short time of 90 s. In the flash sintering treatment, the oxygen vacancies were introduced into zirconia bulk samples through an electrochemical reduction reaction. Furthermore, subgrains with grain boundaries and defects such as dislocations and stacking faults are generated during the flash treatment. The as-prepared ZrO_{2-x} bulk samples exhibited excellent light absorption capacity (> 92%) in the whole solar spectral region due to their small band gap, indicating promising applications in the field of solar energy harvesting. ZrO_{2-x} possessed remarkable photocatalytic activity and it could decompose nearly 89.65% of MB within 100 min. Flash sintering treatment provides a cost-effective, rapid, and environmentally friendly method for production of ZrO_{2-x}. In addition, flash sintering treatment can be applied to other materials to generate large concentrations of oxygen vacancies.

Acknowledgements

This work was financially supported by the National Natural Science Foundation of China (Nos. 52472064 and 12305298), the Open Project of State Key Laboratory of Environmentally-friendly Energy Materials (No. 23kfhg06), the Sichuan Science and Technology Program (No. 2022JDTD0017), and the Natural Science Foundation of Jiangsu Province (No. BK20230864).

Declaration of competing interest

The authors have no competing interests to declare that are relevant to the content of this article.

Electronic Supplementary Material

Supplementary material is available in the online version of this article at https://doi.org/10.26599/JAC.2024.9220976.

References

[1] Chen XB, Liu L, Yu PY, *et al.* Increasing solar absorption for photocatalysis with black hydrogenated titanium dioxide nanocrystals. *Science* 2011, **331**: 746–750.

[2] Sun B, Ouellette O, García de Arquer FP, *et al.* Multibandgap quantum dot ensembles for solar-matched infrared energy harvesting. *Nat Commun* 2018, **9**: 4003.

[3] Wang ZP, Lin ZP, Shen SJ, *et al.* Advances in designing heterojunction photocatalytic materials. *Chin J Catal* 2021, **42**: 710–730.

[4] Pan XY, Yang XH, Yu MQ, *et al.* 2D MXenes polar catalysts for multi-renewable energy harvesting applications. *Nat Commun* 2023, **14**: 4183.

[5] Aldeen EMS, Jalil AA, Mim RS, *et al.* Altered zirconium dioxide based photocatalyst for enhancement of organic pollutants degradation: A review. *Chemosphere* 2022, **304**: 135349.

[6] Emeline A, Kataeva GV, Litke AS, *et al.* Spectroscopic and photoluminescence studies of a wide band gap insulating material: Powdered and colloidal ZrO_2 sols. *Langmuir* 1998, **14**: 5011–5022.

[7] Gionco C, Paganini MC, Giamello E, *et al.* Paramagnetic defects in polycrystalline zirconia: An EPR and DFT study. *Chem Mater* 2013, **25**: 2243–2253.

[8] Nanda B, Pradhan AC, Parida KM. Fabrication of mesoporous CuO/ZrO_2–MCM–41 nanocomposites for photocatalytic reduction of Cr(VI). *Chem Eng J* 2017, **316**: 1122–1135.

[9] Kim M, Lee B, Ju H, *et al.* Oxygen-vacancy-introduced $BaSnO_{3-\delta}$ photoanodes with tunable band structures for efficient solar-driven water splitting. *Adv Mater* 2019, **31**: 1903316.
[10] Ji QQ, Bi L, Zhang JT, *et al.* The role of oxygen vacancies of ABO_3 perovskite oxides in the oxygen reduction reaction. *Energy Environ Sci* 2020, **13**: 1408–1428.
[11] Chen CY, Jiang T, Hou JH, *et al.* Oxygen vacancies induced narrow band gap of BiOCl for efficient visible-light catalytic performance from double radicals. *J Mater Sci Technol* 2022, **114**: 240–248.
[12] Bi X, Du GH, Kalam A, *et al.* Tuning oxygen vacancy content in TiO_2 nanoparticles to enhance the photocatalytic performance. *Chem Eng Sci* 2021, **234**: 116440.
[13] Kim KH, Choi CW, Choung S, *et al.* Continuous oxygen vacancy gradient in TiO_2 photoelectrodes by a photoelectrochemical-driven "self-purification" process. *Adv Energy Mater* 2022, **12**: 2103495.
[14] Qi FG, Yang ZW, Zhang JF, *et al.* Interfacial reaction-induced defect engineering: Enhanced visible and near-infrared absorption of wide band gap metal oxides with abundant oxygen vacancies. *ACS Appl Mater Inter* 2020, **12**: 55417–55425.
[15] Lee YJ, Putri LK, Ng BJ, *et al.* Blue TiO_2 with tunable oxygen-vacancy defects for enhanced photocatalytic diesel oil degradation. *Appl Surf Sci* 2023, **611**: 155716.
[16] Dashtbozorg B, Shi FZ, Tagliaferro A, *et al.* Plasma defect-engineering of bulk oxygen-deficient zirconia. *Acta Mater* 2024, **262**: 119457.
[17] Sinhamahapatra A, Jeon JP, Kang J, *et al.* Oxygen-deficient zirconia (ZrO_{2-x}): A new material for solar light absorption. *Sci Rep* 2016, **6**: 27218.
[18] Zu D, Wang HY, Yang TZ, *et al.* Black ZrO_2 synthesized by molten lithium reduction strategy for photocatalytic hydrogen generation. *J Am Ceram Soc* 2020, **103**: 4035–4042.
[19] Wang Q, Edalati K, Koganemaru Y, *et al.* Photocatalytic hydrogen generation on low-bandgap black zirconia (ZrO_2) produced by high-pressure torsion. *J Mater Chem A* 2020, **8**: 3643–3650.
[20] Cologna M, Rashkova B, Raj R. Flash sintering of nanograin zirconia in < 5 s at 850 °C. *J Am Ceram Soc* 2010, **93**: 3556–3559.
[21] Yang JX, Tan L, Ji PC, *et al.* Rapid preparation of $Gd_2Zr_{2-x}Ce_xO_7$ waste forms by flash sintering and their chemical durability. *J Eur Ceram Soc* 2023, **43**: 4950–4957.
[22] Li YJ, Chi QG, Yan ZY, *et al.* Flash sintering of high-purity alumina at room temperature. *J Adv Ceram* 2023, **12**: 2382–2388.
[23] Liu JL, Xu X, Liu DG, *et al.* Ultrafast formation of Al_2O_3–$Y_3Al_5O_{12}$ eutectic ceramic by flash sintering. *J Am Ceram Soc* 2020, **103**: 4051–4056.
[24] Liu FM, Bai B, Cheng L, *et al.* Rapid synthesis of $Li_4Ti_5O_{12}$ as lithium-ion battery anode by reactive flash sintering. *J Am Ceram Soc* 2022, **105**: 419–427.
[25] Zhu YC, Zhou HY, Huang RX, *et al.* Gas-discharge induced flash sintering of YSZ ceramics at room temperature. *J Adv Ceram* 2022, **11**: 603–614.
[26] Biesuz M, Pinter L, Saunders T, *et al.* Investigation of electrochemical, optical and thermal effects during flash sintering of 8YSZ. *Materials* 2018, **11**: 1214.
[27] Caliman LB, Bouchet R, Gouvea D, *et al.* Flash sintering of ionic conductors: The need of a reversible electrochemical reaction. *J Eur Ceram Soc* 2016, **36**: 1253–1260.
[28] Christian KH, Charalambous H, Jha SK, *et al.* Current-ramp assisted sintering of 3YSZ: Electrochemical and microstructural comparison to flash and thermal sintering. *J Eur Ceram Soc* 2020, **40**: 436–443.
[29] Eqbal A, Chakrabarti T. Study on the electrochemical effect of ZnO addition on flash sintering of 3 mol% yttria stabilized zirconia. *J Eur Ceram Soc* 2023, **43**: 6260–6271.
[30] Alvarez A, Dong YH, Chen IW. DC electrical degradation of YSZ: Voltage-controlled electrical metallization of a fast ion conducting insulator. *J Am Ceram Soc* 2020, **103**: 3178–3193.
[31] Liang YH, Xiang SQ, Zhang XF. Fabrication of highly conducting undoped ZnO ceramics by flash sintering. *J Eur Ceram Soc* 2024, **44**: 5989–5999.
[32] Jo S, Kindelmann M, Jennings D, *et al.* Flash-induced defects in single-crystal 8YSZ characterized by TEM, XRD, and Raman spectroscopy. *J Am Ceram Soc* 2024, **107**: 5786–5800.
[33] Bechteler C, Todd RI. Lattice modification of $ZrO_{2-\delta}$ and formation of rocksalt structure ZrO and Zr(O,N) after DC electrical loading of 3YSZ. *J Eur Ceram Soc* 2024, **44**: 1044–1052.
[34] Zhao XH, Yan NP, Li YJ, *et al.* Dielectric barrier discharge based defect engineering method to assist flash sintering. *J Adv Ceram* 2023, **12**: 1046–1057.
[35] Wu AX, Yan ZY, Wang XL, *et al.* A versatile defect engineering strategy for room-temperature flash sintering. *J Adv Ceram* 2022, **11**: 1172–1178.
[36] Liu JL, Liu DG, Ren K, *et al.* Research progress on the flash sintering mechanism of oxide ceramics and its application. *J Inorg Mater* 2022, **37**: 473–480. (in Chinese).
[37] Raj R. Joule heating during flash-sintering. *J Eur Ceram Soc* 2012, **32**: 2293–2301.
[38] Yadav D, Raj R. The onset of the flash transition in single crystals of cubic zirconia as a function of electric field and temperature. *Scripta Mater* 2017, **134**: 123–127.
[39] Yang JX, Fu MY, Tian Q, *et al.* Preparation of $Gd_2Zr_2O_7$ nanoceramics by flash sintering and two-step flash sintering. *Ceram Int* 2023, **49**: 16594–16602.
[40] Raj R. Analysis of the power density at the onset of flash sintering. *J Am Ceram Soc* 2016, **99**: 3226–3232.
[41] Dong YH, Chen IW. Onset criterion for flash sintering. *J Am Ceram Soc* 2015, **98**: 3624–3627.
[42] Merle T, Guinebretiere R, Mirgorodsky A, *et al.* Polarized Raman spectra of tetragonal pure ZrO_2 measured on epitaxial films. *Phys Rev B* 2002, **65**: 144302.
[43] Naumenko AP, Berezovska NI, Biliy MM, *et al.* Vibrational analysis and Raman spectra of tetragonal zirconia. *Phys Chem Solid State* 2008, **9**: 121–125.
[44] Lv HD, Bao JX, Ruan F, *et al.* Preparation and properties of black Ti-doped zirconia ceramics. *J Mater Res Technol* 2020, **9**: 6201–6208.
[45] Fukushima H, Uchida H, Funakubo H, *et al.* Evaluation of oxygen vacancies in ZnO single crystals and powders by micro-Raman spectroscopy. *J Ceram Soc Japan* 2017, **125**: 445–448.
[46] Zhang JJ, Gao YF, Jia XR, *et al.* Oxygen vacancy-rich mesoporous ZrO_2 with remarkably enhanced visible-light photocatalytic performance. *Sol Energ Mat Sol C* 2018, **182**: 113–120.
[47] Mao YS, Wang PF, Li LN, *et al.* Unravelling the synergy between oxygen vacancies and oxygen substitution in BiO_{2-x} for efficient molecular-oxygen activation. *Angew Chem Int Ed* 2020, **59**: 3685–3690.
[48] Li CQ, Yi SS, Chen DL, *et al.* Oxygen vacancy engineered $SrTiO_3$ nanofibers for enhanced photocatalytic H_2 production. *J Mater Chem A* 2019, **7**: 17974–17980.
[49] Hata JI, Hirayama M, Suzuki K, *et al.* Effect of surface chemical bonding states on lithium intercalation properties of surface-modified lithium cobalt oxide. *Batteries Supercaps* 2019, **2**: 454–463.
[50] Wang JS, Yu YL, Li S, *et al.* Doping behavior of Zr^{4+} ions in Zr^{4+}-doped TiO_2 nanoparticles. *J Phys Chem C* 2013, **117**: 27120–27126.
[51] Xu YY, Liu XN, Guo HX, *et al.* Efficient catalytic transfer hydrogenation of furfural to furfuryl alcohol over Zr-doped ordered mesoporous carbon synthesized by Zr-arbutin coordinated self-assembly. *Fuel* 2023, **331**: 125834.
[52] Azdad Z, Marot L, Moser L, *et al.* Valence band behaviour of zirconium oxide, Photoelectron and Auger spectroscopy study. *Sci Rep* 2018, **8**: 16251.
[53] Yang NN, Shen P, Yang B, *et al.* Significant improvement in the wettability of ZrO_2 by molten Al under the application of a direct current. *Mater Des* 2016, **111**: 158–163.
[54] Lv HF, Zhou YJ, Zhang XM, *et al.* Infiltration of $Ce_{0.8}Gd_{0.2}O_{1.9}$ nanoparticles on $Sr_2Fe_{1.5}Mo_{0.5}O_{6-\delta}$ cathode for CO_2 electroreduction in solid oxide electrolysis cell. *J Energy Chem* 2019, **35**: 71–78.
[55] Li LL, Ji PC, Geng C, *et al.* Facile synthesis of high-entropy

$(Co_{0.2}Cr_{0.2}Fe_{0.2}Mn_{0.2}Ni_{0.2})_3O_4$ nanopowders and their electrochemical properties as supercapacitor electrode. *J Energy Storage* 2023, **73**: 109182.

[56] Cho J, Li Q, Wang H, *et al.* High temperature deformability of ductile flash-sintered ceramics via *in situ* compression. *Nat Commun* 2018, **9**: 2063.

[57] Li J, Cho J, Ding J, *et al.* Nanoscale stacking fault-assisted room temperature plasticity in flash-sintered TiO_2. *Sci Adv* 2019, **5**: eaaw5519.

[58] Janek J, Korte C. Electrochemical blackening of yttria-stabilized zirconia—Morphological instability of the moving reaction front. *Solid State Ion* 1999, **116**: 181–195.

[59] Makuła P, Pacia M, Macyk W. How to correctly determine the band gap energy of modified semiconductor photocatalysts based on UV–Vis spectra. *J Phys Chem Lett* 2018, **9**: 6814–6817.

[60] Qi FG, Yang ZW, Wang Y, *et al.* Defects in black zirconia responsible for solar energy harvesting. *J Mater Chem C* 2021, **9**: 16732–16740.

[61] Heiroth S, Ghisleni R, Lippert T, *et al.* Optical and mechanical properties of amorphous and crystalline yttria-stabilized zirconia thin films prepared by pulsed laser deposition. *Acta Mater* 2011, **59**: 2330–2340.

[62] Bouaniza N, Hosni N, Maghraoui-Meherzi H. Structural and optical properties of Cu_3SbS_3 thin film deposited by chemical bath deposition along with the degradation of methylene blue. *Surf Coat Tech* 2018, **333**: 195–200.

[63] Teeparthi SR, Awin EW, Kumar R. Dominating role of crystal structure over defect chemistry in black and white zirconia on visible light photocatalytic activity. *Sci Rep* 2018, **8**: 5541.